

Ocean circulation and terrestrial runoff dynamics in the Mesoamerican region from spectral optimization of SeaWiFS data and a high resolution simulation

L. M. Chérubin · C. P. Kuchinke · C. B. Paris

Received: 21 May 2007 / Accepted: 11 December 2007
© Springer-Verlag 2008

Abstract The evolution in time and space of terrestrial runoff in waters of the Mesoamerican region was examined using remote sensing techniques combined with river discharge and numerical ocean circulation models. Ocean color SeaWiFS images were processed using a new Spectral Optimization Algorithm for atmospheric correction and ocean property retrieval in Case-2 waters. A total of 157 SeaWiFS images were collected between 1997 and 2006 and processed to produce Colored Detrital Material images of the Mesoamerican waters. Monthly terrestrial runoff load and river discharge computed with a land-elevation model were used as input to a numerical model, which simulated the transport of buoyant matter from terrestrial runoff. Based on land cover for years 2003–2004, modeling results showed that the river discharge seasonality was correlated with the image averaged CDM, and the simulated plume reproduces the spatial patterns and temporal evolution of the observed CDM plume. River discharge peaked in August and CDM peaked from September to January. The buoyant matter

concentration was high from October to January, and was at its lowest from March to April. Between October and December the plume was transported out of the Mesoamerican waters by a cyclonic gyre located north of Honduras. Part of the runoff from Honduras was transported towards Chinchorro Banks and the Yucatan Channel, part re-circulated into the Gulf of Honduras, and part taken toward the outside of the Mesoamerican Barrier Reef System. This study shows that all the reefs of the MBRs, including the most offshore atolls of the region, are under the influence of terrestrial runoff on a seasonal basis, with maximum effect during October to January, and minimum from March to April. Furthermore, what is seen as a giant plume in satellite images is in fact composed of runoffs of different ages.

Keywords Mesoamerican barrier reef system · SeaWiFS · CDM · ROMS · Passive tracer · Terrestrial runoff

Communicated by Biology Editor M.P. Lesser.

L. M. Chérubin (✉)
Division of Meteorology and Physical Oceanography,
Rosenstiel School of Marine and Atmospheric Science,
University of Miami, Miami, FL 33101, USA
e-mail: lcherubin@rsmas.miami.edu

C. P. Kuchinke
Department of Physics, Rosenstiel School of Marine
and Atmospheric Science, University of Miami,
Miami, FL 33101, USA

C. B. Paris
Division of Marine Biology and Fisheries,
Rosenstiel School of Marine and Atmospheric Science,
University of Miami, Miami, FL 33101, USA

Introduction

The Mesoamerican Region (MAR) consists of the oceanic systems off Honduras, Guatemala, Belize and Mexico, and contains one of the largest coral barrier reefs in the Caribbean. Landward, this region has one of the largest watershed networks of the Caribbean, with numerous rivers flowing out to the coastal ocean. Until recently, there has been little research focusing on the factors critical to the conservation of biodiversity hotspots, such as coral ecosystems at the interface between the land and its watershed, and the ocean currents. Land use around the MAR, such as the clearing of native vegetation and its replacement with intensive agriculture and coastal development, has changed the ecological interdependence of forest and waters, such

as the delivery of nutrients through estuaries and the utilization of coastal habitat by marine species. In particular, the transport of pollutants to the coastal ocean has increased to a level many times the natural rate (Wilkinson 1999; McKergow et al. 2005). The altered water quality of streams has led to degradation in the estuaries, coastal waters, and coral reefs. Natural events such as hurricanes in the MAR can induce flooding and extreme river run-offs which reach the offshore coral reef barrier. Andréfouët et al. (2002) and Sheng et al. (2007) showed how the 1,000 km of reefs of the MAR were connected by ocean currents, carrying sediments and nutrients from the land to the oceanic waters during hurricane Mitch. Excessive sediments (suspended or deposited) and elevated nutrients are almost universally recognized as having adverse effects on reef communities (Spalding et al. 2001). The management of coral reef environments, including reef-building and non reef-building communities, would benefit from a greater understanding of the degree of physical connectivity between coral reefs and between land, watershed and offshore reefs through the movement of water masses carrying detrital material (Kleypas et al. 2001).

The MAR is located in the western Caribbean Sea where the Caribbean Current flows from the Nicaraguan Rise westwards towards the Yucatan peninsula, then veers north toward the Yucatan Channel (Richardson 2005). To the north and south lie two regions populated by eddies. In the north, drifter trajectories collected from the Global Drifting Buoy Data Assembly (<http://www.aoml.noaa.gov/phod/dac/dacdata.html>) show the continuous presence of cyclones and anticyclones while to the south, two large cyclones (~100 km diameter) were sampled by drifters (Richardson 2005). However, very few of these drifters entered the MAR, and as a result, in situ observations are limited within this region. The presence of a cyclonic circulation in the Gulf of Honduras was recognized in two numerical simulations (Ezer et al. 2005; Tang et al. 2006). In the latter study, cyclones south of the Caribbean Current were less visible than in Ezer et al. (2005), and the simulated Caribbean Current was more to the south of the MAR (16.5°N) than mean flow obtained from drifter trajectories (18°N; Richardson 2005).

Observations from space-borne sensors have improved spatial information on natural processes. The availability of calibrated satellite ocean color data provides a unique data set that helps explore spatial and temporal patterns of connectivity between land processes and the coastal ocean. Recent developments in bio-optical models contribute to the quantification of suspended particulate matter concentrations (SPM; see Appendix) in coastal waters with an absolute uncertainty <30%. There have been attempts to quantitatively compare SPM fields from images and models (Jorgensen and Edelvang 2000; Durand et al. 2002), but

uncertainty on a number of parameters involved in the SPM transport model prevents their generalization. Satellite ocean color data has been used to explore patterns of connectivity between reefs as well as between reef and land in the MAR (Andréfouët et al. 2002; Sheng et al. 2007), suggesting that pathways for pollutants and pathogens within and among coral reef provinces could be inferred realistically using satellite ocean color observations.

Recent numerical modeling approaches, merged with in situ or remote sensing data analysis, have been effective in studying sediment transport (Ouillon et al. 2004; Blaas et al. 2007; Luick et al. 2007). Together with Geographic Information Systems (GIS), they have improved investigations into how marine and terrestrial environments are related across large spatial and temporal scales.

The goals of this study are to investigate the interactions between river runoff and open water in the MAR, and the extent of the terrestrial influence on coral reefs under various degrees of anthropogenic input. This is achieved by (1) building a 3D hydrodynamic model of the region coupled with a model of river runoff, (2) simulating the transport of suspended sediments and dissolved nutrients (hereafter Buoyant Matter (BM), see Appendix) with various scenarios of land use, and (3) assessing the spatial and temporal linkages of satellite-derived measurements with transport of river runoff to the reef areas.

Material and methods

Study area

A detailed description of the Mesoamerican Barrier Reef System (MBRS) is given in Andréfouët et al. (2002). Briefly, the MBRS extends over 1,000 km (Fig. 1) and includes the Mexican Caribbean reefs and islands along the Yucatan coast, the Belizean atolls and a large barrier reef, and Honduran reefs around the Bay Islands. Guatemala has a very short Caribbean coastline that is heavily influenced by sediment-laden rivers, and thus has negligible coral reefs. The shelf slope along the Belize Barrier Reef is very steep, with depths of 1,000 m existing less than 3 km seaward of the reef crest. The southeastern shelf slope rises more gently such that the Honduran coast is oceanic to the shore (Heyman and Kjerfve 2000).

The Gulf of Honduras is a receiving basin, where terrestrial drainage is distributed by marine processes and impacts ecosystem function. Over 80% of the sediment and half of the nutrients (both nitrogen and phosphorus) delivered by watersheds along the MAR originate in Honduras (Burke and Sugg 2006). Guatemala is also a source of about one-sixth of all sediments and about one-quarter of all nitrogen and phosphorus. In comparison, relatively minor percentages of

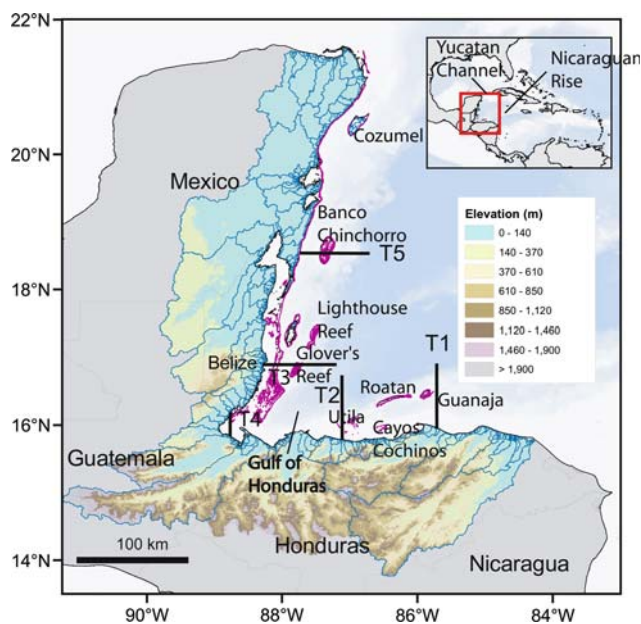


Fig. 1 Mesoamerican Region. Land elevation is shown in color, river network in blue and reefs in magenta. Thick black lines show the location of the transects labeled T number

the regional sediment load come from Belize and Mexico (Burke and Sugg 2006). Belize contributes 10–15% of nutrients and Mexico about 5% of the nutrients. Values for Mexico are probably underestimated as the contribution of underground rivers is not included.

Peak transport of freshwater and fluvial sediments occurs in the wet season from July to October. Wet season discharge usually exceeds dry season discharge by a factor of 5–9 (Heyman and Kjerfve 2000; Burke and Sugg 2006; Fig. 2). According to Heyman and Kjerfve (2000), the flux of freshwater from the high rainfall areas in southern Belize, Guatemala, and Honduras gives rise to easterly flowing, density-driven surface currents that exit the inner Gulf of Honduras. In contrast, and in response to occasional southerly winds, Heyman and Kjerfve (2000) suggest that deep, clear nutrient-rich oceanic waters from the Cayman Trench enter the Gulf flowing westerly.

The three Belizean atolls have been assumed to be outside the general influence of terrestrial runoff. Glovers Reef, the southernmost atoll, is located more than 40 km from the Belize coast and approximately 100 km from the Honduras and Guatemala coasts. Glovers Reef has been used as a control site, based on the assumption that it was free of anthropogenic effects and terrestrial pollutants. For instance, Wilkinson (1987) related sponge biomass to terrestrial runoff along a transect in the Belize barrier reef, and Glovers Reef was used as the lowest influence site even though it was found to have an unexpectedly high biomass of sponges. McClanahan and Muthiga (1998) explicitly considered Glovers to lie beyond terrigenous influence.

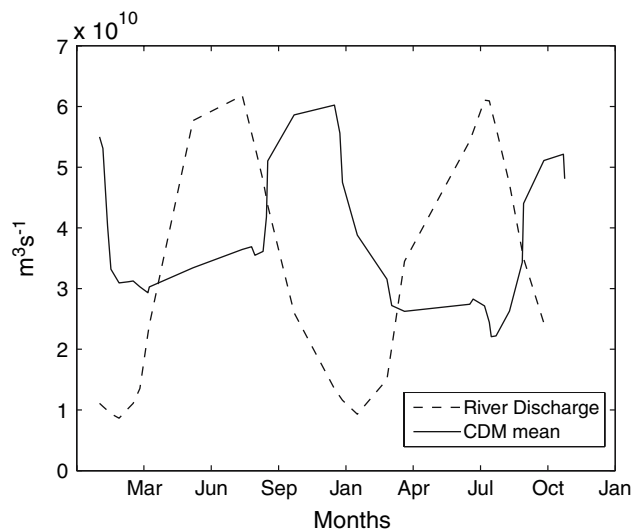


Fig. 2 N-SPECT river discharge (dashed line) overlaid on the image mean CDM absorption coefficient (solid line) from year 2003 to 2004 imagery to show interannual variability. The river monthly discharge time series from Burke and Sugg (2006) is matched to the available day of data of the SOA imagery, which creates a distortion in the discharge profile

Ocean color data processing

Visible and near infrared (NIR) radiance in this study was obtained from the passive Sea-viewing Wide Field-of-view Sensor (SeaWiFS) on board the SeaStar polar orbiting satellite. Data was processed using the latest available calibration of the sensor. A major component of the current NASA ocean color retrieval procedure is to retrieve the aerosol properties, including optical depth and diffuse transmittances, on a pixel by pixel basis, using a comparison of the spectral variation between the two measured NIR bands and a suite of scattering-only aerosol models. This aerosol information is then interpolated across visible wavelengths and removed from the total measured radiance (Gordon and Wang 1994). The remaining water leaving spectral radiance $L_w(\lambda)$ can then be used in a variety of empirical bio-optical models to obtain information on chlorophyll concentration C (e.g., O'Reilly et al. 1998). In this study the standard ocean color algorithm (Gordon and Wang 1994) was replaced with an alternate Spectral Optimization Algorithm (SOA). This algorithm contains a suite of absorbing aerosol models and a semi-analytic Case 2 bio-optical algorithm, both important for coastal environments.

The SOA bio-optical model (Garver and Siegel 1997; Maritorena et al. 2002), herein referred to as GSM, retrieves both C and $a_{\text{CDM}}(443)$, the absorption coefficient of Colored Detrital Material (CDM) at 443 nm. Here, $a_{\text{CDM}}(443) = a_{\text{dp}}(443) + a_{\text{CDOM}}(443)$, the sum of the respective absorption due to detrital particles and colored

dissolved organic matter, respectively. They are combined due to their similar spectral signatures. As a general rule, a_{CDM} in offshore waters may contain 80–90% a_{CDOM} with the remainder being a_{dp} . For waters very near to the coast the % of a_{CDOM} may decrease to as low as 40% (e.g., Chesapeake Bay in Magnuson et al. 2004). GSM spectral-slope coefficients have not been developed for the coast of Belize and Honduras. This would require optimization of GSM with extensive in situ data collected at the ocean surface. Instead, a developed set of coefficients from the Santa Barbara Channel, CA, were used. Sensitivity analyses showed that for CDM, use of incorrect coefficients in coastal waters introduced an absolute error of less than 10–20%, decreasing rapidly as we increase CDM. Relative error is considered much less. Since CDM and detrital particles are components of DOC and POC respectively (see Appendix) it is proposed that the spatial and temporal trends in a_{CDM} can be used as a surrogate for *Buoyant Matter* (BM) in this study. From herein $a_{\text{CDM}}(443)$ is referred to as CDM.

The SeaWiFS sensor has been operational since October 1997. A search of the entire SeaWiFS archive of High Resolution Picture Transmission (HRPT) scenes was undertaken up to June 2006 to evaluate the best images. The coastlines of Belize and Northern Honduras are very cloudy for most of the year, with the months of October to March displaying, on average, about two clear days per month. For the months of April to September there are few cloud free days. For example, from May to July only two usable cloud-free scenes were found in the entire archive 1997–2006. To maintain a processing data set of sufficient size it was decided to accept images that contained at least 80% of clear sky for at least the first 50 km of ocean bounding the East coast of Belize and the entire Northern coast of Honduras. The filtering procedure resulted in 157 images from 1997 to 2006 for both Chlorophyll and CDM. Most scenes were processed for 15.5°N–18.5°N; 81.0°W–89.0°W, corresponding to an approximately square region bounded by the bottom half of the East coast of Belize and the entire Northern coast of Honduras. Few scenes displayed clear skies along the entire East coast of Belize. Hence for these scenes the processing was extended to latitude 23.0°N.

From the nine year dataset, only 157 days could be used to build what we assume is climatological time series. This was obtained by a weighted average of CDM in order to account for the number of data per year. CDM were averaged for each month to account for the varying number of days per month. Because the years 2003 and 2004 were the most complete, they were used along with the mean to compute a standard deviation of CDM variability. In order to compare SOA data with numerical model outputs, SOA images were projected on a constant-space grid. Values on

transects perpendicular to the coast were then extracted to build time series, and surface averaged CDM values for each image were calculated in order to build a time series of the global CDM content in the Mesoamerican region (Fig. 2).

This method justifies the lag observed in Fig. 2 as the changes are dependent on the CDM in the entire domain and not only in coastal waters. In this study no attempt was made to estimate the BM concentration from the CDM absorption coefficient. Only the relative variation between consecutive days was considered and this was compared with values from a similar spatial and temporal analysis of numerical model results. Figure 2 illustrates that CDM is a good proxy for the terrestrial runoff transport since CDM exhibits seasonal changes, which correlate with the river discharge.

Numerical modeling

The Regional Ocean Modeling System (ROMS) is a 3D hydrodynamic model, which simulates the spatial and time evolution of ocean state variables and current. The model domain is the wider Gulf of Honduras, which encompasses the eastern coast of the Yucatan Peninsula and the northern coast of Honduras (15.5–21.3°N, 89.1–84.3°W). It includes the barrier reef, reef lagoon, and adjacent oceanic waters and uses a 1 km resolution bathymetry from the World Resources Institute (<http://www.wri.org/>). The horizontal resolution of the simulation is 2 km and the model has 25 vertical layers. Model variables of the ocean state (temperature, salinity) at the open ocean boundaries were relaxed to the monthly Levitus ocean (<http://ingrid.ideo.columbia.edu/SOURCES/LEVITUS94/>) climatology (World Ocean Atlas). Tides were set at the boundary by the TPXO6 global tide model (http://www.esr.org/polar_tide_models/Model_TPXO62_load.html). Monthly varying surface fluxes (wind, rain, solar, radiative heat fluxes, evaporation) were obtained from the Comprehensive Ocean Atmosphere Dataset (<http://icoads.noaa.gov/>) (COADS) climatology.

The river discharge and sediment load (used as a proxy for suspended sediments and dissolved nutrients) in over 400 watersheds that discharge adjacent to the Mesoamerican barrier reef were provided by the Non-point Source Pollution and Erosion Comparison Tool (N-SPECT) developed by the US National Oceanographic and Atmospheric Administration (NOAA), whose results are analyzed in Burke and Sugg (2006). N-SPECT results were validated by comparing river discharge and terrestrial runoff load with in-situ data in several regions around the world. Note Buoyant Matter (BM) is used in the ROMS model as a substitute for suspended and dissolved material

here. Burke and Sugg (2006) used scenarios of land cover change in the MAR until 2025 to evaluate the impact of land cover change on river discharge, sediment and pollutant delivery. Two land use scenarios were tested in this study: the first one is called the *Current Year* scenario, based on land cover of years 2003–2004. The second one, called *Sustainability First* scenario, which could result in a 3–4% decline in nutrients and transported sediment to the MAR.

During the *Current Year* scenario, Burke and Sugg (2006) examined the relative accumulation of sediment and nutrients at river mouths across the MAR. The Ulua watershed (Honduras) appeared as the largest contributor of sediment, nitrogen, phosphate, and total suspended solids. Other large contributors of sediment and nutrients were the Rio Patuca (Honduras), Rio Motagua (in Guatemala and Honduras), Aguan (Honduras), Rio Dulce (Guatemala), Belize River watershed (Belize), and Tinto o Negro (Honduras).

BM load from the 400 watersheds was modeled as a passive tracer by advection and diffusion. The diffusion coefficient for all the simulations was fixed to $10 \text{ m}^2 \text{ s}^{-1}$. Each river discharge and BM load provided by the N-SPECT model was individually entered into the model domain for each month and kept constant for each month. The BM inputs then follow the seasonal changes due to rainfall and their spatial variability. Rivers were defined as point sources of tracers with an exponential vertical distribution on the vertical. The higher inflow was in the upper layer. The model did not simulate resuspension and deposition of fine suspended sediments, which are known to deposit in the first few hundred meters from estuaries, whereas dissolved nutrient matter can spread much further (Devlin and Brodie 2005). Therefore, the model produces a climatology of the circulation and BM transport in the Mesoamerican coastal and offshore waters, and reefs. In order to reach passive tracer balance the model was first operated for a year and subsequently reached its BM equilibrium in January of the second and third year. Two simulations are then compared, each one using run-off inputs from the two land use scenarios described in Burke and Sugg (2006). Moreover initial conditions for the *Sustainability First* scenario were taken from hurricane flooding event.

The accuracy of the MAR circulation in the ROMS simulation coupled to the N-SPECT output was estimated by first comparing seasonal variations of the plume dispersion patterns with the CDM dispersion patterns. A more detailed comparison was undertaken by analyzing the extent and evolution of time series of CDM and BM along five transects perpendicular to the shore around the region. Transects 1 and 2 are meridional, extending over one degree of latitude west of Guaraja (85.7°W) and across

Utila Reef (87°W), north of Honduras. Transect 3 is zonal and crosses Belize's lagoon and reefs at $17^\circ.13\text{N}$. Transect 4 is meridional and crosses the Gulf of Honduras from Guatemala to Belize. Transect 5 is zonal (1° of longitude wide), and runs across Chinchorro Bank (Fig. 1).

Results

Satellite colored detrital material versus N-SPECT river discharges

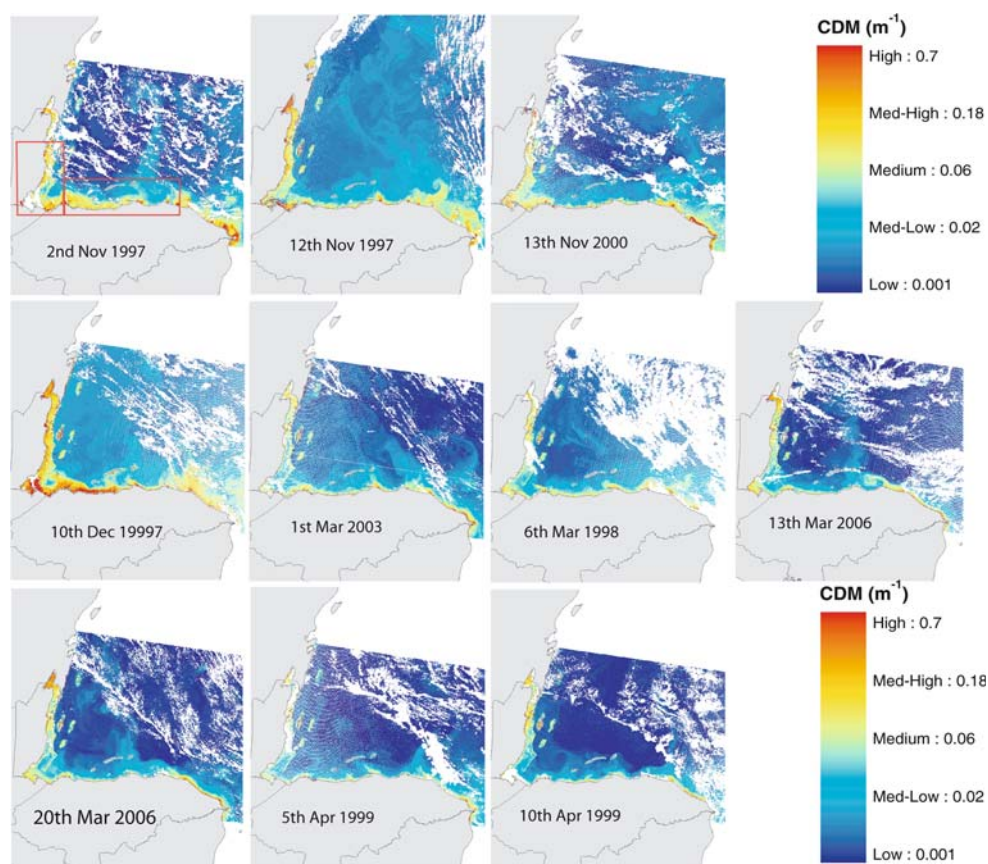
A 173-day lag was found between the increase of the river run-off in March and the increase of CDM concentration in September over the entire MAR (Fig. 2). Colored detrital material concentration peaks on average 2–3 months (September–December) after the peak in river run-off (June–August). From one year to the next, this cycle repeats itself. When the river discharge is minimum in March–April, CDM content has been expelled from the MAR and reaches its minimum from July to September. This time lag is likely to be different in coastal waters, which are under the direct influence of the runoff.

Seasonal evolution of the colored detrital material concentration in the MAR

In order to analyze the seasonal variability of the CDM spatial patterns, images were clustered by season. Due to the limited number of clear days available, only October–December, January–March, and April were identified. Based on the river run-off seasonality (Fig. 2), one may expect to see an increase in the CDM concentration on-shore and to some extent off-shore, in the days and months following the run-off maxima, which are September, October, November, December and perhaps January of the next year. Lowest month run-off should yield a limited spreading of CDM and the lowest concentrations, from April to June.

The highest concentration of CDM along the coast occurs between October and December through offshore transport by filaments. From November to December, the concentration in coastal waters is increasing and filaments are observed in the eastern Gulf of Honduras due to the entrainment by the mesoscale circulation from the east of the Honduras Peninsula (Fig. 3). Later in December, high concentrations onshore are seen in the western Gulf and are moved offshore by filaments north of the coastal waters of Honduras (Fig. 3). A remnant plume offshore shows the advection of CDM from Honduras heading northwest toward Banco Chinchorro (Fig. 3, 1 March 2003; 6 March 1998) and reveal the presence of a cyclonic gyre carrying

Fig. 3 Times series of CDM absorption coefficient (m^{-1} , high values *red*, low values *blue*) in the MAR where the same month of different years is shown for year to year consistency. Color scale is logarithmic. *Red boxes* on 2 November 1997 image show the regions where CDM was spatially averaged to produce the times series of Fig. 8



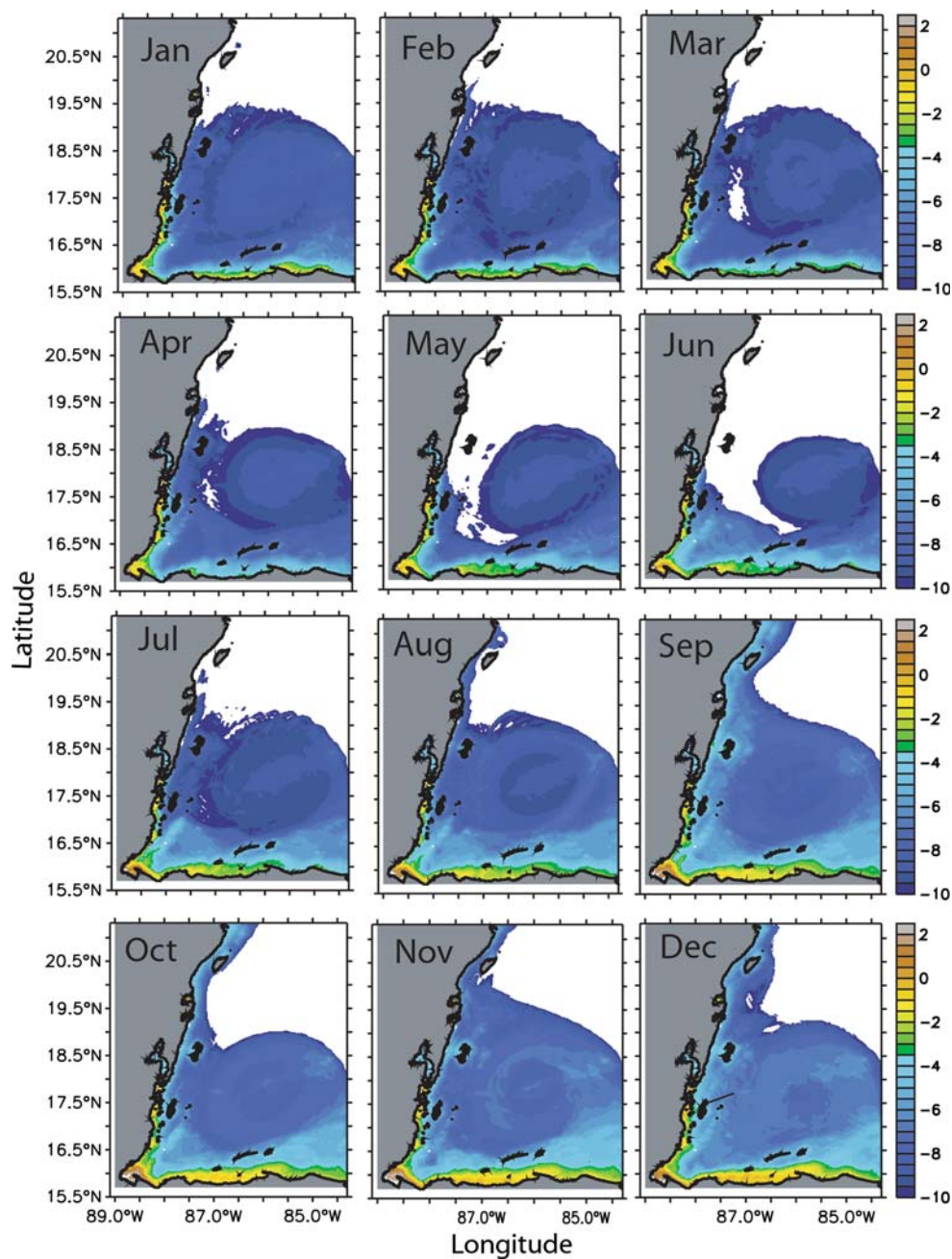
CDM from eastern Honduras west north-west toward the coast of Mexico. From January to March the CDM concentration has decreased in coastal waters of Honduras whereas concentrations are still high in the Belize coastal waters (Fig. 3, 1 March 2003–20 March 2006). The barrier reef seems to prevent the circulation of mesoscale flow in the coastal waters, as seen in Honduras waters. Offshore dispersion continues by small filaments along the Honduras coast. Later in March, clear waters in the gyre are observed and short filaments continue to expel CDM from the coast of Honduras (Fig. 3, 13 March 2006; 20 March 2006). In April the weakest concentrations are seen onshore with small filaments still contributing to the expelling of CDM from Honduras coastal waters towards open waters (Fig. 3, 5–10 April 1999). Concentration has also decreased in the Belize Coastal waters.

Mesoamerican region dynamics in the ROMS model

The climatology of the model circulation in the MAR is characterized by the presence of a semi-permanent cyclonic gyre in the monthly mean (Fig. 4). This gyre extends from the Belize offshore waters to about 85°W , north of Honduras. It carries coastal waters from this region of

Honduras northwards toward the Chinchorro Banks. Most of the year, the current south of 18.5°N flows southward in the channel between the coast and Chinchorro Bank (87.7°W , 18.3°N , Fig. 5a). This result differs from Ezer et al.'s (2005) model at the same location. However, further north (87.5°W , 18.7°N , Fig. 5b) the ROMS simulation shows a similar seasonal variability to the Ezer et al. (2005) simulation at 87.7°W , 18.3°N . From January to March the flow is southward, then reverses northward in March–April, July, and August–September, and southward in May–June and from October to December. Some recirculation cells, cyclonic or anticyclonic, are observed in the Gulf of Honduras but their life time is limited to a few days. Model time series at the eastern side of Lighthouse Reef (84.7°W , 17.13°N) show the high variability of the meridional component of the current. The seasonal variability with peaks of northward velocity from January to March and in May is similar to the estimated altimeter velocity near Lighthouse Reef in Ezer et al. (2005). Further east on the Honduras coast, model currents flow eastward carrying coastal waters from Belize toward Honduras. Nonetheless, cross-shore filaments entrained by small scale eddies contribute to the offshore advection of coastal waters as seen in the CDM imagery (Fig. 3). The cyclonic gyre can be damped by the influence of the large scale

Fig. 4 ROMS monthly mean of passive tracer concentration (kg m^{-3} , high values *brown*, low values *blue*) for the current year scenario simulation. The color scale is logarithmic



Caribbean Current that will flow directly toward the coast of Mexico and turn north in the Gulf of Honduras in place of the cyclonic gyre. This is the dominant feature in Ezer et al.'s (2005) model and the cyclonic gyre is smaller and centered in the Gulf of Honduras. Based on their Fig. 10, the gyre eastward extension reaches $87\text{--}86^\circ\text{W}$. In the CDM imagery (Fig. 3) the gyre extends to 86°W for instance in November 1997, March 1998, but also to 85° in November 2000 and March 2003. North of 19°N , current flows northward along the coasts of Mexico as observed in drifter trajectories by Richardson (2005). Therefore most of the BM delivered by Mesoamerican watersheds is transported

out of the region as a result of the northward flow from the eastern Honduras waters to the coast of Mexico. Then the BM is taken north into the Yucatan Channel mostly in October–December (Fig. 4).

Analysis of the changes between the current and sustainability-first scenarios

There was less sediment load for the *Sustainability First* scenario than for the *Current Year* scenario (Fig. 6). However the initial state for the *Sustainability First*

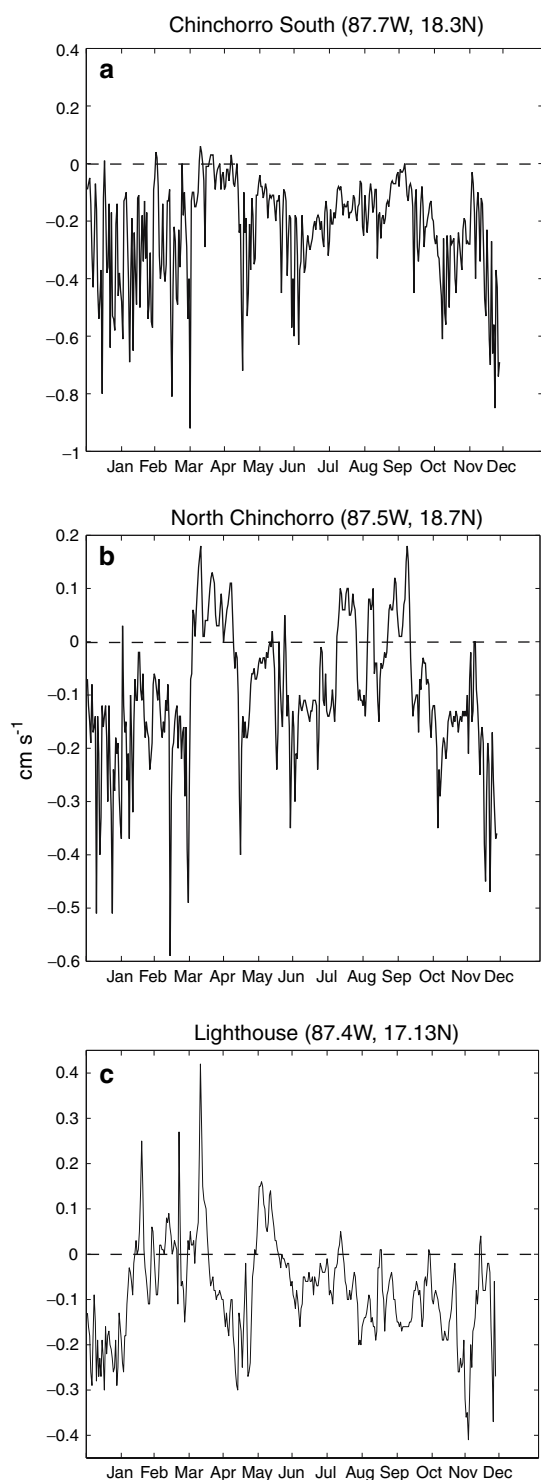


Fig. 5 ROMS surface current time series in the channel between Mexico and Chinchorro Bank, a south at 87.7°W, 18.3°N, b north at 87.5°W, 18.7°N, and c east of Lighthouse Reef (87.4°W, 17.13°N)

scenario was taken from a flooding scenario simulation, which contains globally more BM than the *Current Year* in January (Fig. 7a). Consequently, BM remains in the region for longer during the *Sustainability First* scenario

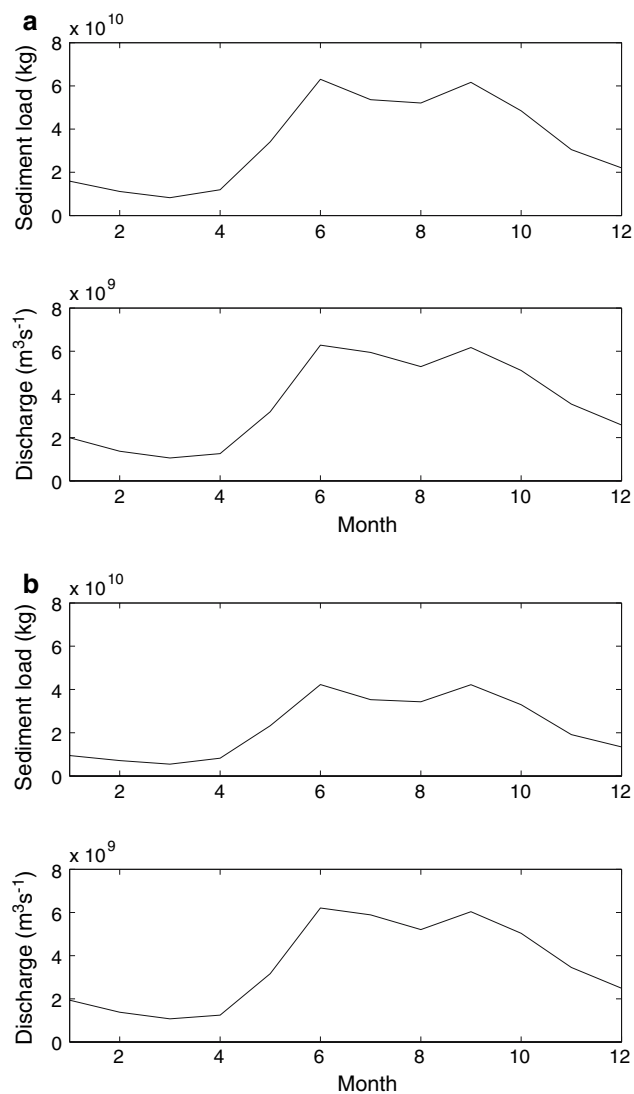


Fig. 6 Time series for the entire coastline of the sediment load (kg, upper plot) and discharge ($\text{m}^3 \text{s}^{-1}$) from the NSPECT model for the current year (a) and the sustainability first (b) scenarios

simulation even though the sediment load is lower (Fig 7b, c). No interruption is seen in the transport out of the MAR of BM between Chinchorro Banks and the Yucatan Peninsula. The difference between the two simulations is detailed in the analysis of the time series of the model transects.

Seasonal buoyant matter changes on transects

Both the numerical model and the CDM data were used to track the BM plume along the MAR coasts. A very similar behavior to the CDM in the SeaWiFS data (Fig. 2) was obtained in the model BM plume seasonal evolution. The

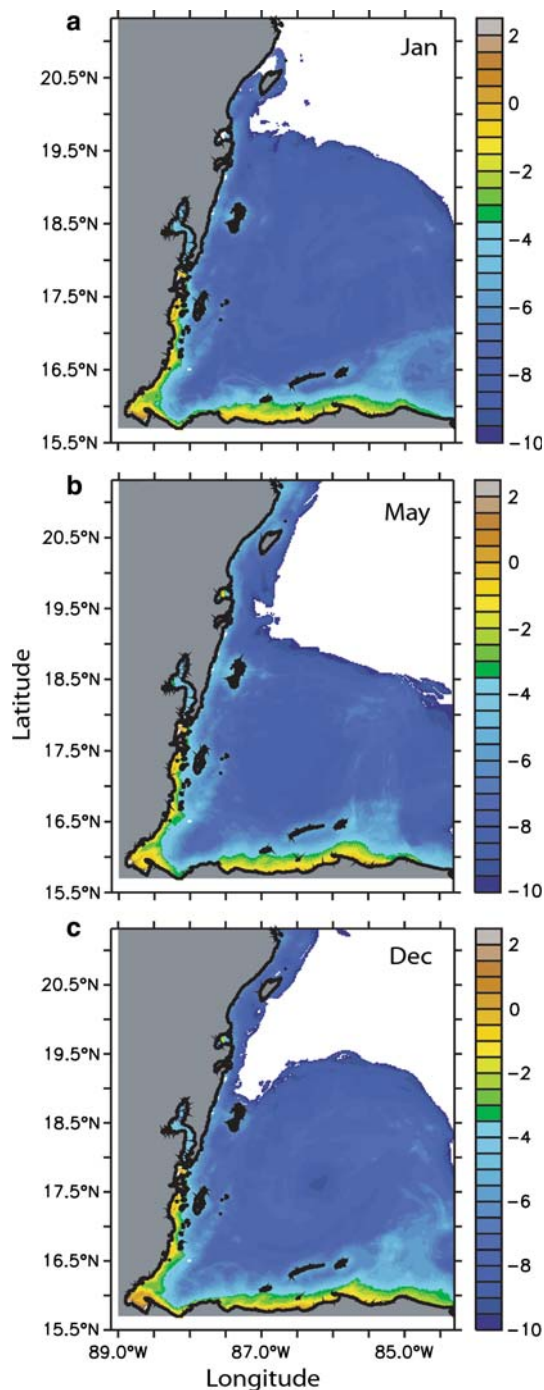


Fig. 7 ROMS monthly mean of sediment concentration (kg m^{-3} , high values *brown*, low values *blue*) for January (a), May (b) and December (c) in the Sustainability First scenario. Color scale is logarithmic

maximum of BM content in the MAR model was obtained during the months of October–December with a peak in September (Fig. 8a). In the real data, the peak time varies with location and most likely from one year to the other. A peak in CDM absorption coefficient was seen in September 2003 in the Gulf of Honduras (Fig. 8b) and later in

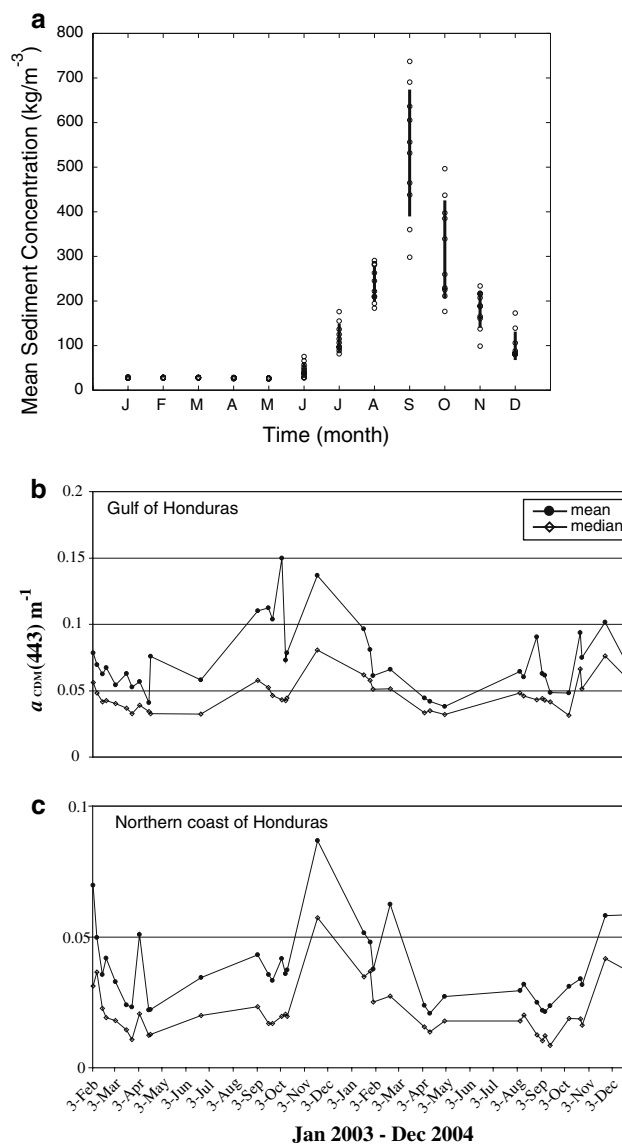


Fig. 8 a Time series of the ROMS mean BM concentration for the current year scenario. Each *circle* corresponds to a day and the bar shows the standard deviation (kg m^{-3}). b Mean (*dot*) and median (*open diamond*) of the surface averaged CDM time series in the Gulf of Honduras from Feb. 2003 to Dec. 2004 calculated in the *left red box* shown in the first frame of Fig. 4. c Same as b on the northern coast of Honduras (*right red box* on the first frame of Fig. 4

November 2003 on the northern coast of Honduras (Fig. 8c), after being averaged in their respective box shown in Fig. 3. The same lag was seen in 2004.

Here the CDM time series for the climatological year, and years 2003 and 2004 are compared with both the *Current Year* and the *Sustainability First* scenarios along the five transects defined previously. Years 2003 and 2004 are used in this comparison because they contained most of the variability seen in the nine year dataset (not shown). Time series for each ~ 1 km resolution (1 pixel) transects of the mean CDM at 0–12 km (coastal), 13–24 km

(inshore), 25–36 km (shelf), 39–50 km (shelf slope) and 50–70 km (off-shore) were computed.

Transect 1

Figure 9a, b shows the time series of mean CDM averaged at different locations along the transect as defined above. As seen in the images (Fig. 3), CDM was higher along the coast year long; CDM decreased from January to April, and

increased from October to December. There were maxima in January and from October to December and minima in April–May. However, these extremes were subject to interannual variability as shown by the times series from 2003 and 2004. CDM decreased from coastal to offshore waters in general. In shelf slope and offshore waters, CDM peaked in February rather than in January in more coastal waters, whereas it peaked earlier between October and December in offshore waters than in coastal waters. Therefore, expelling of runoff is faster in offshore waters

Fig. 9 Transect 1, **a** SOA CDM climatology averaged in 0–12 km (coastal, blue), 13–24 km (inshore, red), 25–36 km (shelf, black) strips. **b** Same as (a) in 39–50 km (shelf slope, blue) and 50–70 km (off-shore, black) strips. Stars and crosses show the standard deviation associated with years 2003 and 2004. **c** Same as (a) for the BM concentration in the Current Year scenario. **d** Same as (b) for the BM concentration in the Current Year scenario. **e** Same as (c) for the Sustainability First scenario. **f** Same as (d) for Sustainability First scenario

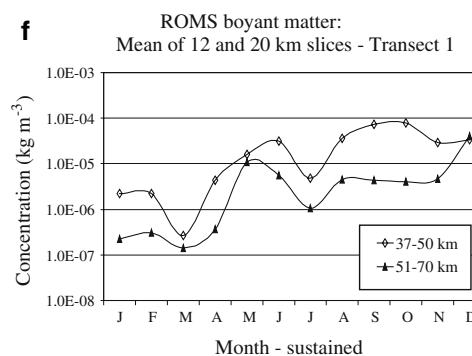
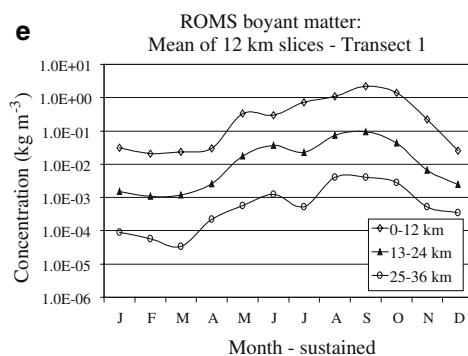
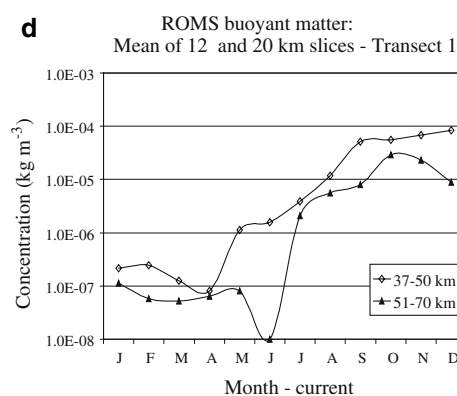
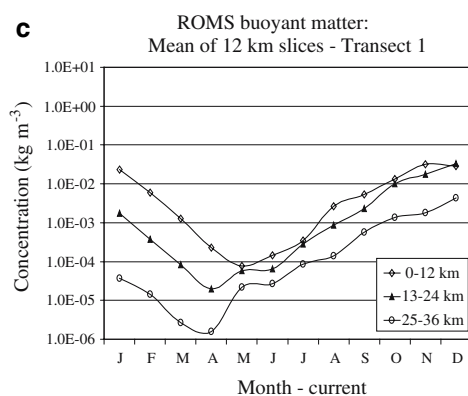
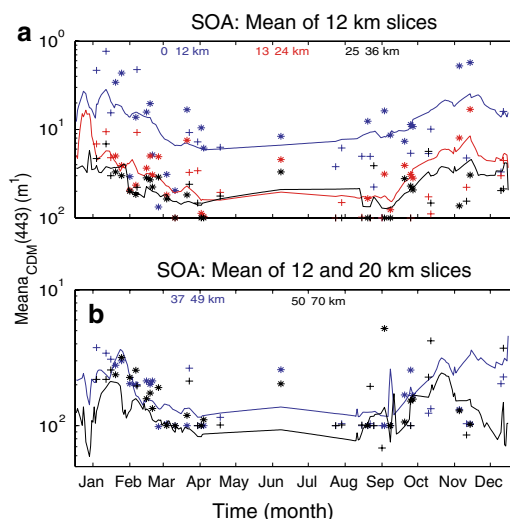
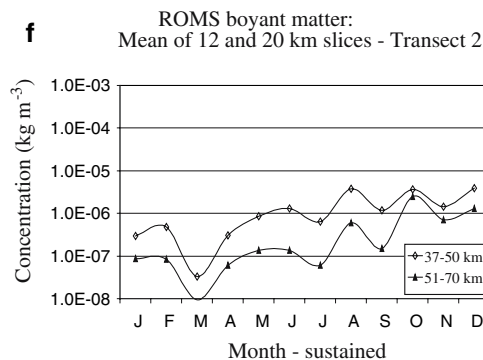
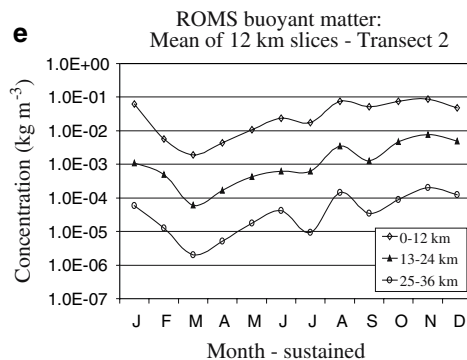
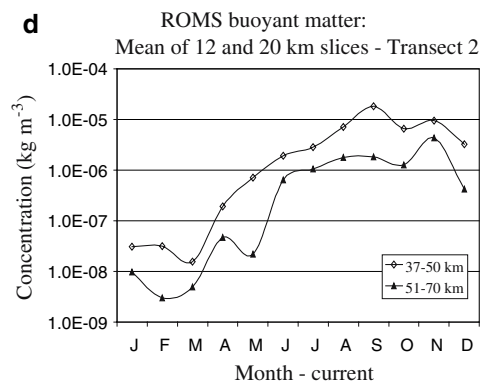
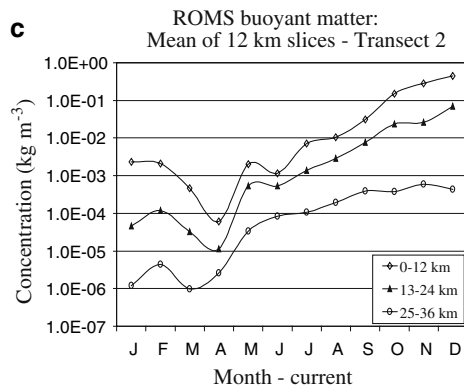
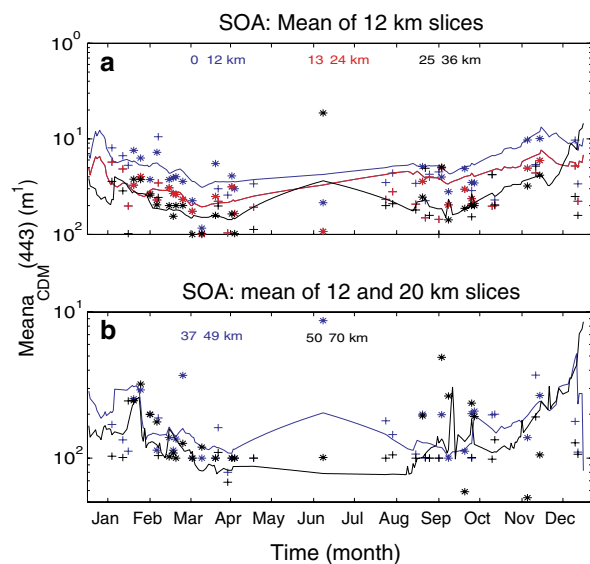


Fig. 10 Transect 2, **a** SOA CDM climatology averaged in 0–12 km (coastal, *blue*), 13–24 km (inshore, *red*), 25–36 km (shelf, *black*) strips. **b** Same as (a) in 39–50 km (shelf slope, *blue*) and 50–70 km (off-shore, *black*) strips. Stars and crosses show the standard deviation associated with years 2003 and 2004. **c** Same as (a) for the BM concentration in the Current Year scenario. **d** Same as (b) for the BM concentration in the Current Year scenario. **e** Same as (c) for the Sustainability First scenario. **f** Same as (d) for Sustainability First scenario

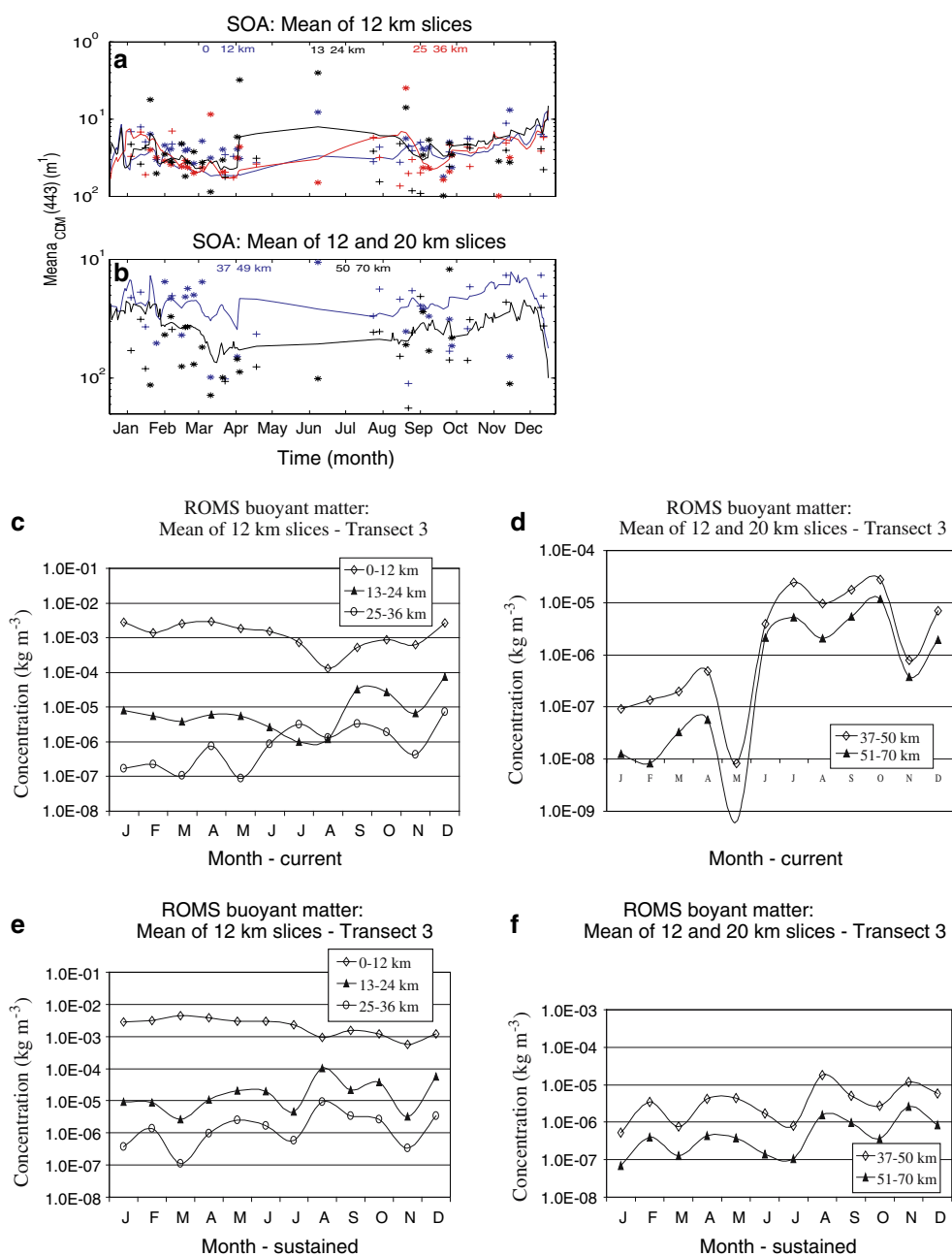


than in coastal waters, as it remains there for less time (Fig. 9b).

In the ROMS model (Fig. 9c, d), the same trends were seen during the *Current Year* simulation. BM concentration peaked between October and December and was at the lowest in April–May. On the shelf slope and offshore, the BM concentration rapidly increases from April to September. This was an artifact of the transport to offshore waters of terrestrial run-off input over shallower regions

during January–February maxima. During the *Sustainability First* scenario (Fig. 9e, f), the initial presence of high BM concentration contributes to an increased mean of the BM concentration. In contrast to the *Current Year* simulation, BM concentration decreased from October to December after a peak in September. In both scenarios the concentration decreased from coastal to offshore waters. However, the change was not so drastic between January–March and April–June in the *Sustainability First* scenario

Fig. 11 Transect 3, **a** SOA CDM climatology averaged in 0–12 km (coastal, *blue*), 13–24 km (inshore, *red*), 25–36 km (shelf, *black*) strips. **b** Same as (a) in 39–50 km (shelf slope, *blue*) and 50–70 km (off-shore, *black*) strips. *Stars* and *crosses* show the standard deviation associated with years 2003 and 2004. **c** Same as (a) for the BM concentration in the Current Year scenario. **d** Same as (b) for the BM concentration in the Current Year scenario. **e** Same as (c) for the Sustainability First scenario. **f** Same as (d) for Sustainability First scenario



(on the shelf slope and offshore, although the transport to offshore waters starts earlier, in March here). In both scenarios, the shelf slope and offshore waters have a slightly different seasonality than in the observations. Instead of having two periods of runoff expelling, they exhibit only one, starting in April and lasting till October.

Transect 2

Seasonal changes in the first three strips were smaller than those found at Transect 1, and although the same

trends were observed (Fig. 10a, b) the gradient across the plume was weaker. In offshore waters, seasonal changes were larger compared to Transect 1. Transport to offshore waters occurred in February, and also possibly from July to November. Retention in offshore waters appeared to take place after October as CDM rapidly increases.

In the model time series, the plume gradient was sometimes larger than at Transect 1 for the *Current Year* scenario (Fig. 10c, d). However, changes between January and June were smaller compared to Transect 1 but the maximum was higher in October–December. Transport to

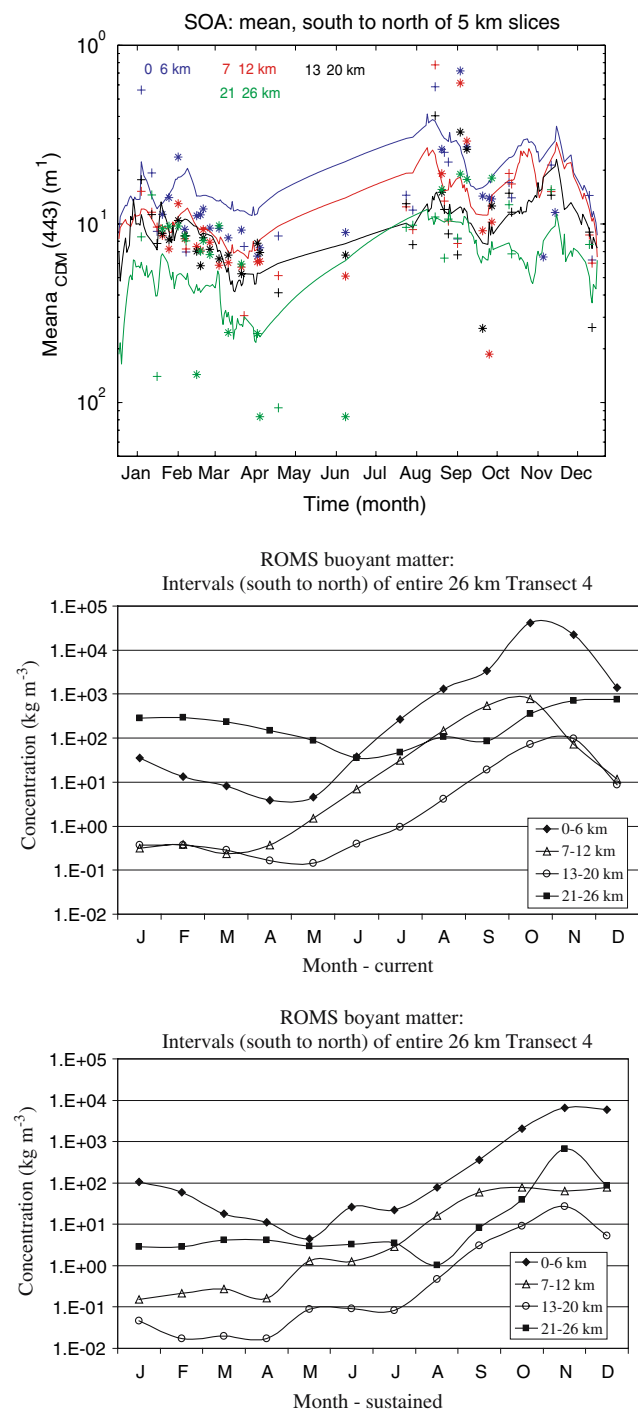


Fig. 12 Transect 4. **a** SOA CDM climatology averaged in 0–6 km (coastal, blue), 7–12 km (red, inshore), 13–20 km (shelf slope, black), and 21–26 km (offshore, green) strips. **b** Same as (a) for the BM concentration in the Current Year scenario. **c** Same as (b) for the Sustainability First scenario

the shelf slope and offshore waters started earlier than at Transect 1, between April and June, and peaked from July to November. For the *Sustainability First* scenario, the gradient across the plume was larger but BM concentration

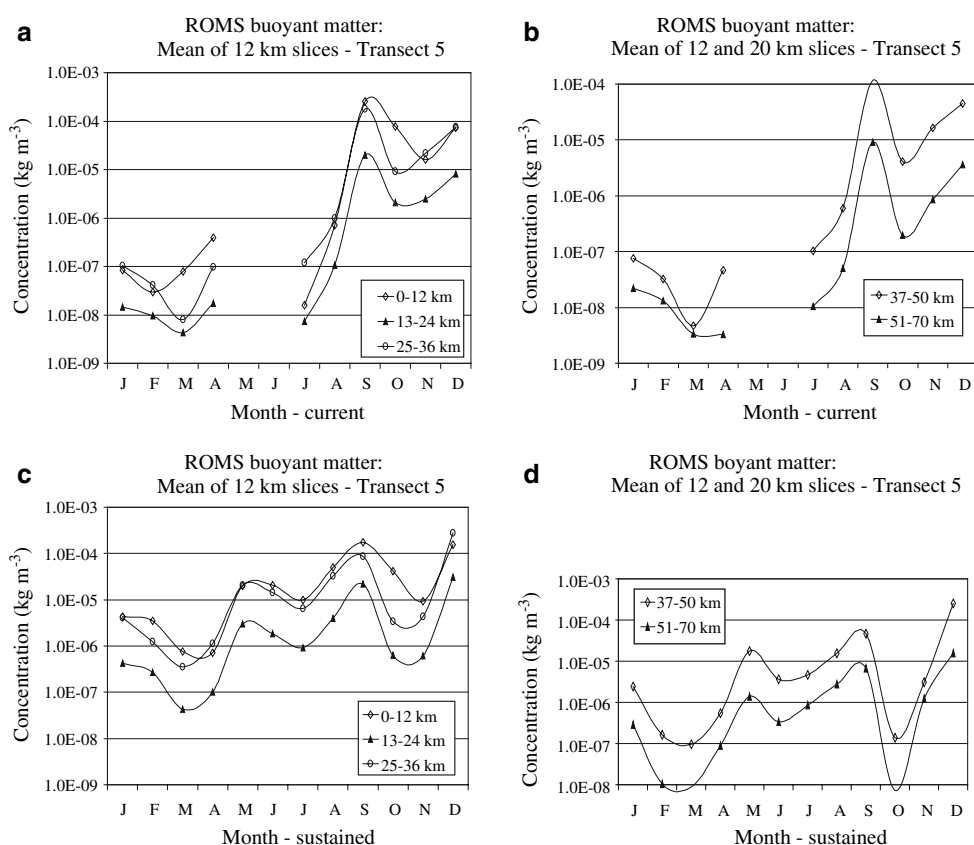
changes were smaller than for the *Current Year* scenario (Fig. 10e, f). In addition, transport to shelf slope and offshore waters was not as significant as Transect 1 (Figs. 9f, 10f). As at Transect 1, the seasonality of the shelf slope and offshore waters differed between the model and the observations, yet July–September expelling could realistically occur (Fig. 10b). To summarize, changes at Transect 2 were smaller than at Transect 1 in offshore waters as in the SOA retrievals.

Transect 3

Strip widths defined for this transect were such that the coastal and inshore strips are inside the Belize Barrier Reef (BBR) and the shelf one outside this reef. Contrary to Transect 1, CDM varied slightly between January and March in coastal waters, and rose from April–December (Fig. 11a). Inshore waters showed a strong increase in April. Monthly river discharge time series (Fig. 6) showed that a rise in coastal waters CDM coincided with a rise in river discharge after April. Shelf water exhibited a maximum in August followed by a drop in September–October and later, a slow rise. However, on the shelf slope and offshore, seasonal variations were larger than in coastal waters. Offshore waters here exhibited the same seasonal variability as the same waters on Transects 1 and 2 (Fig. 11b).

BM concentration in the *Current Year* scenario showed a much higher concentration in coastal waters than elsewhere (Fig. 11c). The difference between inshore and shelf waters was not as large but still significant (an order of magnitude). Seasonal changes were weaker than on Transects 1 and 2 and the lowest variability was seen in coastal waters, in agreement with the SOA retrievals. Inshore water exhibited a minimum in August, earlier than in the satellite retrievals. On the shelf, which is in the vicinity of the BBR, BM concentration increased after May, dropped in August, and peaked in December, again as in the retrievals. On the shelf slope and offshore, seasonal changes were larger than inside and just outside of the BBR (Fig. 11d). Although the seasonal variations were different from observations in January–March, they were similar between July and December (Fig. 11d). Variations seemed to be independent of the BM regime in coastal waters, as expected due to the presence of the BBR. In the *Sustainability First* scenario, the same concentration difference between coastal and non-coastal waters, and the same opposite trend between coastal and offshore waters were obtained (Fig. 11e, f). In the latter, seasonal changes were not as large as in the *Current Year* scenario.

Fig. 13 Transect 5. **a** BM concentration in the Current Year scenario averaged in 0–12 km (coastal), 13–24 km (inshore), and 25–36 km (shelf) strips. **b** Same as (a) in 39–50 km (shelf slope) and 50–70 km (off-shore) strips. **c** and **d** Same as (a) and (b) for the Sustainability First scenario



Transect 4

This transect crosses the Gulf of Honduras, from Honduras to Belize (Fig. 1) and exhibited the highest CDM coefficient of all transects. Variations were strong over the year and the plume exhibited strong seasonally varying monotonic cross gradients (Fig. 12a). CDM was always higher toward Guatemala than toward Belize. Minima were observed in April of both years and CDM peaks sharply in August and September (Fig. 12a).

In the ROMS scenarios, BM concentrations in the different strips were the highest of all transects and followed the same seasonal changes, in both scenarios, as in the observations (Fig. 12b, c). Concentrations were higher towards Guatemala than near Belize between July and November. Maxima were obtained between October and December, as in the observations. Gradients across the plume were not monotonic, and minima were observed in waters between the two coasts (Fig. 12b, c).

Transect 5

Transect 5 is parallel to transect 3 and extends across Chinchorro Bank where the transport of runoff by the gyre

along the coast of Mexico (toward the Yucatan Channel) takes place (Figs. 3, 4). Since very few clear days were available in this region only the model results are described here. BM concentrations were of the same order of magnitude in all strips between January and March, but lower than the other transects. Later, between July and December, concentration was the highest between the Bank and the coast (Fig. 13a) than offshore (Fig. 13b). Nonetheless, in that passage, BM concentration was higher in coastal waters on both sides of the passage with a minimum in the middle (Fig. 13a). The model showed an absence of BM in the region between April and June for the *Current Year* scenario. Minima were obtained between January and March. BM concentrations peaked in September, three months after the peak in offshore waters along Transect 3 (Fig. 11d). This suggests that the BM transport in the vicinity of Transects 3 and 5 is not subject to the same variability and current dynamics. Between September and December, the BM concentration oscillated with a relative minimum (maximum) in October (December). In the *Sustainability First* scenario, seasonal changes were weaker and no absence of BM was noticed during the year (Fig. 13c, d). The general trend showed an oscillatory increase of the BM concentration over the year in all waters with relative maxima in January, March, September and

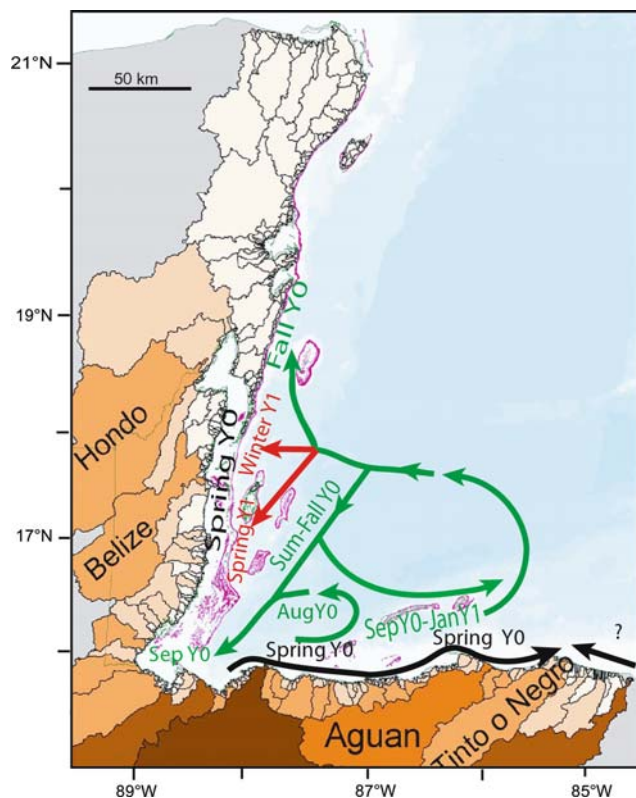


Fig. 14 Summary of the time evolution of the terrestrial runoff dispersion pattern in the MAR superimposed on the annual delivery per basin from Burke and Sugg (2006). Black arrows show the coastal transport, green the offshore circulation patterns and red the remainder of the past year

December. As in the *Current Year*, BM concentration was the highest on the shallow sides of the passage (Fig. 13c). During this scenario, BM transport toward the Yucatan Channel was continuous over the entire year.

Discussion

Due to the time series gaps in clear sky ocean color images that prevail in cloudy tropical areas, numerical simulations calibrated with realistic data could be an alternative to understand the impact of continental runoff to the MBRS. Only few recent studies (Andréfouët et al. 2002; Sheng et al. 2007) have addressed this issue by using SeaWiFS images to track the high concentration runoff plume after hurricane Mitch landfall in November 1998. They were able to show that the atolls and inshore reef are within reach of terrestrial runoffs, and that they have been periodically influenced, mostly during the rainy season. Most of the seasonality of terrestrial runoff in coastal, inshore, shelf, shelf slope, and offshore waters is driven by the seasonality of the river discharge. This in turn is driven by the rainfall, land use and land topography, resulting in soil

erodibility (Burke and Sugg 2006). The use of the ROMS simulation of passive tracer in the MAR proved effective to address the dynamics of terrestrial runoff and its seasonality. The general circulation pattern of terrestrial runoff was compiled with the analysis of time series of both CDM (a_{CDM}) and BM (Fig. 14). Based on these results, the maximum terrestrial runoff content in the MAR occurs between October and January (Figs. 2,8). Minima are obtained in early April after runoffs have been transported out of the MAR. Soon after the beginning of the rainy season (June–July), river discharge reaches the coastal and inshore water of Belize, Guatemala and Honduras. Along the Honduras coast, the plume runoff drifts eastward and spreads northward through filaments (Fig. 3). Maximum concentration in eastern shelf, shelf slope and offshore waters of Honduras occurs between October and December, arriving in September and leaving in January of the next year. The diluted runoff is entrained northwestward toward the MBRS south of Chinchorro Bank, which is also reached between October and December. Some of this diluted runoff re-circulates into the cyclonic gyre, while some is entrained slowly toward the south of BBR, just offshore in Belize's waters. This explains the late increase of runoff concentration outside the BBR between January and March, while it remains almost constant inside (Fig. 11a,b). Some of the runoff in western offshore Honduras waters re-circulates spreading seaward west of the Bay Islands and into the Gulf of Honduras, which contains significant eddy mesoscale activity (not shown). The western corner of the Gulf of Honduras exhibits the highest concentration of terrestrial runoff, which peaks in September. Within the BBR, seasonal changes are not as large as offshore. However, the maximum runoff concentration peaks slightly between October and December as well. This suggests that runoff expelling occurs at a slower rate inside the BBR than in Honduras waters. Moreover the southwestern corner of the Gulf of Honduras appears as a retention area due to the mesoscale eddies.

Figure 14 shows a schematic of the spatial and temporal evolution of the runoff plume in the MAR. It might look like a giant synoptic plume from space but is in fact composed of runoff of different ages. The results of this study show that all the reefs of the region are connected by the terrestrial runoff transport. This connectivity is not only related to special events such as hurricanes (Andréfouët et al. 2002; Sheng et al. 2007) but occurs on a regular basis each year. Therefore any change in the landscape around the MAR will induce changes in the vicinity of most of the reefs of the MBRS at different times of the year.

Comparison between *Current Year* and *Sustainability First* scenarios with CDM imagery of years 2003–2004 reveals that inter-annual variability in the CDM seasonal

cycle can be driven by events in the previous year that will impact the following year until the excess of terrestrial runoff is expelled from the region. Reducing the runoff discharge contributes to lower BM content in coastal waters after one year (Fig. 8c). This result leads to the impact of hurricane activity to the MAR, which could take a year before being dissipated. This finding is also critical for management questions.

Model limitations

As shown by the comparison between the ROMS model and the SOA time series, the behavior of the plumes is not exactly reproduced by the ROMS, most likely because the ROMS is a climatology with smooth seasonal trends and no strong wind or rainfall events. This difference is certainly increased in shallow regions where the ROMS has a minimum constant depth of five meters imposed by the resolution and the constraint of stability of numerical schemes. Shallower minimum depth would require a much higher resolution especially where the depths changes are large. The BBR, which lies at the edge of the shelf drop was not explicitly represented because of the ROMS resolution and the lack of topographic data. However, drop offs at the shelf prevent cross shelf exchanges by nature (Huthnance 2004), explaining why the ROMS simulates without them the presence of the BBR. Other physical processes such as the contribution of sediment deposition and resuspension were not accounted for in this study and most likely contributed to the discrepancies between ROMS and the SOA-processed observations. Also, due to the few clear images available for the entire dataset, comparison with the model climatology needs to be viewed with a degree of caution. Numerous gaps in the dataset prevented an accurate comparison with the model's climatology. Finally, the lack of a defined relationship between the CDM absorption coefficient and the CDM concentration makes estimation of terrestrial runoff concentration from satellite imagery difficult. Direct measurements from water samples, which are not available yet, are necessary to get such information.

These results can be applied to study pollutant transport towards and across the reefs, which in this study are shown to lie in the path of the runoff circulation repeatedly every year. Using marine population connectivity techniques, the stress level of the MBRS due to terrestrial runoff could be examined in order to assess better land-use scenarios as studied by Burke and Sugg (2006).

Acknowledgments This MAR modeling project was jointly funded by the World Resources Institute (WRI) and The Nature Conservancy

(TNC). The authors are grateful to Laretta Burke (WRI), Nestor Vindevoxel (TNC) and Alejandro Arrivillaga (TNC) for providing the funding; to Villy Kourafalou for sharing computer resources at the Rosenstiel School of Marine and Atmospheric Sciences (RSMAS) for this project, and to Johnathan Kool (RSMAS) for technical assistance with GIS processing. C.Paris was also funded by the World Bank/GEF Coral Reef Target Research Program.

Appendix

River water transported to the oceans can be thought of as being made up of, in addition to water, a number of components:

1. PIC (Particulate Inorganic Carbon) = Al, Fe, Si, Ca, K, Mg, Na and P. Alternate names: suspended inorganic matter; sediment. The terms *sediment* is ambiguous. It implies deposition which is dependent on velocity, density and salinity.
2. Dissolved major species, comprising elements with no gaseous phase in the atmosphere (e.g., Cl^- , Na^+ , HCO_3^- , Mg^{2+} , K^+) and elements with gaseous phases (e.g., SO_4^{2-} , HCO_3^-), with the latter derived from atmospheric gases (egg., SO_2 and CO_2 , respectively), as well as from rocks.
3. Dissolved nutrient elements N, P (and sometimes Si), which are used biologically and whose concentrations vary due to this.
4. DOC (Dissolved Organic Carbon). Alternate name: dissolved organic matter. This is primarily sourced from soils and plants.
5. POC (Particulate Organic Carbon) = phytoplankton and detritus (plant material). Alternate name: suspended organic matter.
6. Dissolved trace metals.
7. Suspended trace metals.

From the above list, Suspended Particulate Matter (SPM) will contain PIC, POC and suspended trace metals, the *suspended* terms.

Buoyant Matter will contain ALL terms; however the amount of PIC will depend on the rate of deposition and re suspension from the source.

The ROMS model will invariably replicate the transport of *Buoyant Matter*.

The SOA model produces CDM, the absorption coefficient of Colored Detrital Material. This is comprised of two components

1. The absorption coefficient of colored dissolved organic matter (CDOM), one component of DOC.
2. The absorption coefficient of detrital particles, one component of POC.

Therefore the spatial and temporal trends in CDM can be used as a surrogate for *Buoyant Matter*.

References

- Andréfouët S, Mumby PJ, McField M, Hu C, Muller-Karger FE (2002) Revisiting coral reef connectivity. *Coral Reefs* 21:43–48
- Blaas M, Dong C, Marchesiello P, McWilliams JC, Stolzenbach KD (2007) Sediment-transport modeling on Southern California shelves: a ROMS case study. *Cont Shelf Res* 27:832–853
- Burke L, Sugg Z (2006) Hydrologic modeling of watersheds discharging adjacent to the Mesoamerican Reef. On the watershed analysis for the Mesoamerican Reef, WRI/ICRAN. http://www.wri.org/biodiv/pubs_description.cfm?pid=4256
- Devlin MJ, Brodie J (2005) Terrestrial discharge into the great barrier reef lagoon: nutrient behavior in coastal waters. *Mar Pollut Bull* 51:9–22
- Durand N, Fiandrino A, Fraunie P, Ouillon P, Forget P, Naudin JJ (2002) Suspended matter dispersion in the Ebro ROFI: an integrated approach. *Cont Shelf Res* 22:267–284
- Ezer T, Thattai DV, Kjerfve B, Heyman WD (2005) On the variability of the low along the Meso-American barrier reef system: a numerical model study of the influence of the Caribbean current eddies. *Ocean Dynam* 55:458–475
- Garver SA, Siegel DA (1997) Inherent optical property inversion of ocean color spectra and its biogeochemical interpretation: 1 time series from the Sargasso Sea. *J Geophys Res* 102:18607–18625
- Gordon HR, Wang M (1994) Retrieval of water-leaving radiance and aerosol optical thickness over the oceans with SeaWiFS: a preliminary algorithm. *Appl Optics* 33:443–452
- Heyman WD, Kjerfve B (2000) The Gulf of Honduras. In: Seeliger U, Kjerfve B (eds) *Coastal marine ecosystems. Marine ecosystems of Latin America*. Springer, Berlin, pp 17–32
- Huthnance JM (2004) Ocean to shelf signal transmission: a parameter study. *J Geophys Res* 109:C12029. doi:10.1029/2004JC002358
- Jorgensen PV, Edelvang K (2000) CASI data utilized for mapping suspended matter concentrations in sediment plumes and verification of 2D hydrodynamic modeling. *Int J Remote Sens* 21:2247–2258
- Kleypas JA, Buddemeier RW, Gattuso JP (2001) The future of coral reefs in an age of global change. *Int J Earth Sci* 90:426–437
- Luick JL, Mason L, Hardy T, Furnas MJ (2007) Circulation in the great barrier reef lagoon using numerical tracers and in situ data. *Cont Shelf Res* 27:757–778
- Magnuson A, Harding LW Jr, Mallonee ME, Adolf JE (2004) Bio-optical model for Chesapeake Bay and the middle Atlantic bight. *Estuar Coast Shelf Sci* 61:403–424
- Maritorena S, Siegel DA, Peterson AR (2002) Optimization of semi-analytical ocean color model for global scale applications. *Appl Optics* 41:2705–2714
- McClanahan T, Muthiga N (1998) An ecological shift in a remote coral atoll of Belize over 25 years. *Environ Conserv* 25:122–130
- McKergow LA, Prosser IP, Hughes AO, Brodie J (2005) Regional scale nutrient modeling: exports to the Great Barrier Reef world heritage area. *Mar Pollut Bull* 51:186–199
- O'Reilly JE, Maritorena S, Mitchell BG, Siegel DA, Carder KL, Garver SA, Kahru M, McClain C (1998) Ocean color chlorophyll algorithms for SeaWiFS. *J Geophys Res* 103:24937–24953
- Ouillon S, Douillet P, Andréfouët S (2004) Coupling satellite data with in situ measurements and numerical modeling to study fine suspended-sediment transport: a study for the lagoon of New Caledonia. *Coral Reefs* 23:109–122
- Richardson PL (2005) Caribbean Current and eddies as observed by surface drifters. *Deep Sea Res II* 52:429–463
- Sheng J, Wang L, Andréfouët S, Hu C, Hatcher BG, Muller-Karger FE, Kjerfve B, Heymans WD, Yang B (2007) Upper ocean response of the Mesoamerican barrier reef system to hurricane Mitch and coastal freshwater inputs: a study using SeaWiFS ocean color data and a nested-grid ocean circulation model. *J Geophys Res* 112:C07016. doi:10.1029/2006JC003900
- Spalding M, Ravilious C, Green EP (2001) *World atlas of coral reefs*. University of California Press, Berkeley
- Tang L, Sheng J, Hatcher BG, Sale PF (2006) Numerical study of circulation. Dispersion, and hydrodynamic connectivity of surface waters on the Belize shelf. *J Geophys Res* 111:C01003. doi:10.1029/2005JC002930
- Wilkinson CR (1987) Interocean differences in size and nutrition of oral reef sponge populations. *Science* 236:1654–1657
- Wilkinson CR (1999) Global and local threats to coral reef functioning and existence: review and predictions. *Mar Freshw Res* 50:867–878